A Simple Model of Cortical Intraregional Metastability

Siva Venkadesh[1, *], Asmir Shaikh[2], Heman Shakeri[3,4], Teague R. Henry[1,3],

Ernest Barreto[5], John D. Van Horn[1,3]

[1]*Department of Psychology, University of Virginia, Charlottesville, VA – 22904*
[2]*Department of Computer Science, University of Virginia, Charlottesville, VA – 22904*
[3]*School of Data Science, University of Virginia, Charlottesville, VA – 22904*
[4]*Biomedical Engineering, University of Virginia, Charlottesville, VA – 22904*
[5]*Department of Physics and Astronomy, George Mason University, Fairfax, VA – 22030*

*Correspondence: si9xr@virginia.edu

Abstract:

Transient synchronization of bursting activity in neural networks, which occurs in patterns of metastable phase relationships between neurons, is a notable feature of network dynamics observed *in vivo*. However, the mechanisms that contribute to this dynamical complexity in neural circuits are not well understood. Local circuits in cortical regions consist of populations of neurons with diverse intrinsic oscillatory features. In this study, we numerically show that the phenomenon of transient synchronization, also referred to as metastability, emerges in an inhibitory neural population when the neurons' intrinsic fast-spiking dynamics are appropriately modulated by slower inputs from an excitatory neural population. Using a compact model of a mesoscopic-scale network consisting of excitatory pyramidal and inhibitory fast-spiking neurons, our work demonstrates a relationship between the frequency of neural oscillations and the features of emergent metastability. In addition, a novel metric is formulated to characterize collective transitions in metastable networks. Finally, we discuss potential applications of our compact representation of mesoscopic network metastability in modeling whole-brain resting-state dynamics using empirically estimated anatomical connectivity.

Keywords: transient attractors, itinerancy, bursting dynamics, emergent complexity, network connectivity

Introduction

Computational modeling of cortical dynamics that incorporates mesoscopic-scale connectivity features can offer a powerful framework for investigating neural network mechanisms in normal and pathological conditions (Venkadesh & Van Horn, 2021). However, current approaches for modeling the mesoscopic-scale dynamics of brain regions (Kopsick et al., 2022; Markram et al., 2015) are limited by the lack of an integrative concept (Frégnac, 2017) that coherently unifies the multitude of mechanisms that are present in real neural networks. This is primarily due to limited theoretical accounts for the emergent dynamical complexities in a network in terms of its constituent mechanisms.

An empirically observable complexity *in vivo* is the metastable attractor dynamics at the level of individual neurons. More specifically, a neuron can exhibit bursting oscillations that transiently synchronize with the oscillations of other neurons, and these synchronizations can occur at different phases of oscillations (Ego-Stengel & Wilson, 2007; Jones & Wilson, 2005; Lisman, 2005; Poe et al., 2000; Skaggs & McNaughton, 1996; Vinck et al., 2010). In other words, biological neural networks can realize a range of attractor states that are locally observable through different phase-locking modes between individual neurons. Such transient attractor dynamics are also referred to as metastability or itinerancy, and this phenomenon is hypothesized to be a necessary physical property underlying the coordinated dynamics between spatially distant neural populations (Tognoli & Kelso, 2014). Moreover, a moment of conscious experience is hypothesized to exist irresolvably for the duration between successive attractor transitions in the brain (W. J. Freeman, 1999).

The mathematical conditions for the emergence of transient dynamics have been previously discussed (Tsuda, 2009). More recently, conduction delays between brain areas were associated with metastable oscillations on a macroscopic spatial scale (Cabral et al., 2022). However, the biophysical features of neural networks underlying metastability at the level of neurons have not been fully elucidated. While a previous work reported metastable attractor dynamics among intrinsically bursting neurons (Venkadesh et al., 2020), it was unclear if metastability could also be realized in neural populations in which bursting dynamics are induced externally. Here, we explore the emergence and characteristics of metastability in a fast-spiking interneuron population that exhibits bursting dynamics due to driving inputs from a population of slower pyramidal neurons. We also examine the quantitative characteristics of collective transitions between attractor states realized in different metastable networks. Finally, we discuss potential applications of our work in modeling the whole-brain resting-state dynamics to understand network physiology in neurodegenerative disorders.

Methods

Neural networks consisting of 100 pyramidal and 50 fast-spiking neurons were constructed using Izhikevich neurons (Izhikevich, 2003) (Equations 1 – 3). The parameters $a, b, c,$ and d (Equations 2 – 3) were selected to match the intrinsic dynamics of each type of neuron. Specifically, these were set to 0.02, 0.2, -65, and 8 respectively for the pyramidal neurons, and 0.1, 0.2, -65 and 2 for the fast-spiking neurons (Izhikevich, 2003).

$$\frac{dv}{dt} = 0.04v^2 + 5v + 140 - u + I^{ext} + I^{syn} \quad (1)$$

$$\frac{du}{dt} = a(bv - u) \quad (2)$$

$$if\ v \geq 30mV, \begin{cases} v = c \\ u = c + d \end{cases} \quad (3)$$

$$I^{syn} = \sum_{i=1}^{m_j} \delta_i \cdot \mathrm{w} \quad (4)$$

coupling scheme (Equation – 4), where each presynaptic spike either increased (excitatory) or decreased (inhibitory) the postsynaptic current by the weight parameter ($\mathrm{w} = +0.3$ for excitatory connections and -0.3 for inhibitory connections). In equation – 4, δ_i is the delta function, which equals one when neuron i spikes and is zero otherwise. The network parameters were chosen to allow pyramidal neurons to induce sustained bursting activity in the inhibitory fast-spiking population for a range of external input currents in the former (I^{ext} in equation – 1). I^{ext} was always set to zero for the fast-spiking neurons. All networks were simulated using Brian2 (Stimberg et al., 2019) for a duration of 10s with a timestep of 0.1ms. Following the network simulation, a low-pass filter was applied to the voltage signal of each neuron (v in Equation – 1) to extract the bursting oscillations without the individual spikes (**Fig. 1C top**). Then, instantaneous phases of the bursting oscillations were assigned to each neuron via Hilbert transform. **Fig. 1C bottom** shows two representative examples.

To assess the nature of network-wide phase relationships, phase differences were computed between pairs of neurons over time. Since time is discrete (with a resolution of 0.1ms), this resulted in an ensemble of phase difference measurements between all possible distinct pairs of neurons ((50*49)/2=1225 pairs) at each time point over the entire duration (10s). Thus, this ensemble consisted of N=122,500,000 phase difference measurements, i.e., angles. Henceforth these angles will be referred to as $\phi_j,\ j = 1,2,\ldots,N$. Then, we constructed the

Network connections were configured as illustrated in **Fig. 1A**. Inter- and intra-population connections were determined randomly with probabilities 0.4 and 0.7, respectively. Post-synaptic effects were specified using an instantaneous pulse-

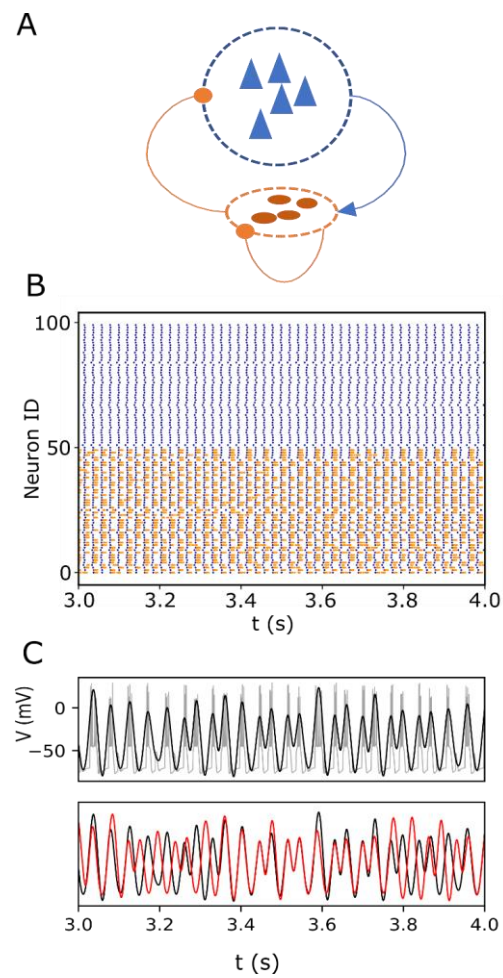

Figure 1. A. Network configuration consisting of pyramidal neurons (blue triangles) and fast-spiking neurons (dark orange ovals). Connections indicated by the arrowhead and circles denote excitatory and inhibitory pulse-coupling, respectively. **B.** Raster plot showing spiking activity in pyramidal (blue) and fast-spiking neurons (orange) for one second. **C.** (top) Bursting activity (gray) in one representative fast-spiking neuron. The filtered signal, superimposed in black, captures the burst oscillations. (bottom) Burst oscillations of two representative neurons (black and red) showing transitions between in- and anti-phase transiently locked modes.

Kuramoto-Daido order parameters Z_n (Daido, 1996; Golomb & Hansel, 2000; Venkadesh et al., 2020):

$$Z_n = \frac{1}{N}\sum_{j=1}^{N} e^{in\phi_j} \tag{5}$$

for n, a positive integer. These order parameters characterize clustering patterns in the ensemble of phase differences. For example, if each ensemble member is plotted as a point on the unit circle in the complex plane at angle ϕ_j, then Z_1 is the centroid of the ensemble. Of interest is the magnitude $|Z_1|$, which ranges from zero to one. If all points occur at the same angle, then $|Z_1| = 1$. In contrast, if the points are scattered uniformly about the unit circle, then $|Z_1| = 0$. Note, however, that if the ensemble of points forms uniformly spaced clusters, then $|Z_1| = 0$. Such arrangements can be identified using the order parameters Z_n with $n > 1$. For example, if the phases form three ideal clusters (i.e., equally populated clusters 120 degrees apart), then $|Z_1| = |Z_2| = 0$, but $|Z_3| = 1$. In fact, for ideal states consisting of c uniformly spaced and equally populated clusters, $|Z_{jc}| = 1$ for any integer $j \geq 1$ and is zero otherwise. To correct for this redundancy, a real-valued quantity G_n was defined, as in equation 6, such that G_n is close to 1 only when the ensemble approximates an ideal n-cluster state.

$$G_n = |Z_n| \times \prod_{j=1}^{n-1}(1 - |Z_j|) \tag{6}$$

To assess the nature of transitions between synchronized states in different metastable networks, the following steps were carried out: The networks were simulated twice with identical initializations. The first simulation was used to establish the baseline clustering of neurons at any given time (i.e., clustering of neurons based on their instantaneous phases). In the second simulation, a fraction of randomly selected interneurons was simultaneously perturbed by single spikes at a certain timepoint. This caused some of the neurons to change their cluster assignments relative to the baseline. Phase cluster assignments of neurons were obtained using Gaussian mixture models (Pedregosa et al., 2011). To quantify the effect of the perturbation, we measured the similarity of the two clustering arrangements of neurons between the baseline and perturbed conditions over time (Equations 7 – 9). Here, RI is "rand index," which measures the similarity of two sets of instantaneous phase clusters, and g and h are the numbers of pairs of neurons with the same and different cluster assignments across two groupings (i.e., number of agreements between two groupings). nC_2 denotes the number of possible combinations of neuron pairs. Thus, the RI for two identical groupings of a set of neurons is one. The adjusted rand index (ARI) (Hubert & Arabie, 1985; Rand, 1971; Steinley, 2004) (Equation – 8) was used to account for chance, and it ensures that the similarity of two random groupings of a set of neurons will be zero. This is achieved by estimating an expected RI ($E(RI)$ in Equation – 8) using random permutations of cluster assignments.

$$RI = \frac{g + h}{nC_2} \tag{7}$$

$$ARI = \frac{RI - E(RI)}{\max(RI) - E(RI)} \tag{8}$$

$$Collective\ response = 1 - \min_{[t_p, t_p + \Delta t]}\{ARI\} \tag{9}$$

The ARIs were measured in 50 simulation trials, each with a random subset of perturbed interneurons and a random time (>0.5s) at which the perturbation was delivered. The minimum observed ARI following the perturbation corresponded to the maximum effect of the perturbation. We defined collective response as in Equation – 9 to characterize the extent to which the system as a whole responds to exogeneous perturbations of a fraction of its elements. For instance, if there is no change to the network state following the perturbation, then the collective response is zero. On the other hand, if a perturbation results in new phase clusters that are equivalent to completely random cluster assignments for all the neurons compared to the baseline condition, then the collective response is one. In Equation – 9, t_p denotes the time at which the perturbations were delivered, and Δt was 1s.

Finally, collective response characteristics were examined in metastable networks for various numbers of perturbed neurons. It is worth mentioning here that while each presynaptic spike influences the activity of a postsynaptic neuron (see Equation 4) on a timescale of a few milliseconds, the collective response aims to characterize activity that is spatiotemporally coarse-grained (i.e., transitions that occur among a group of neurons on a timescale of roughly tens or hundreds of milliseconds).

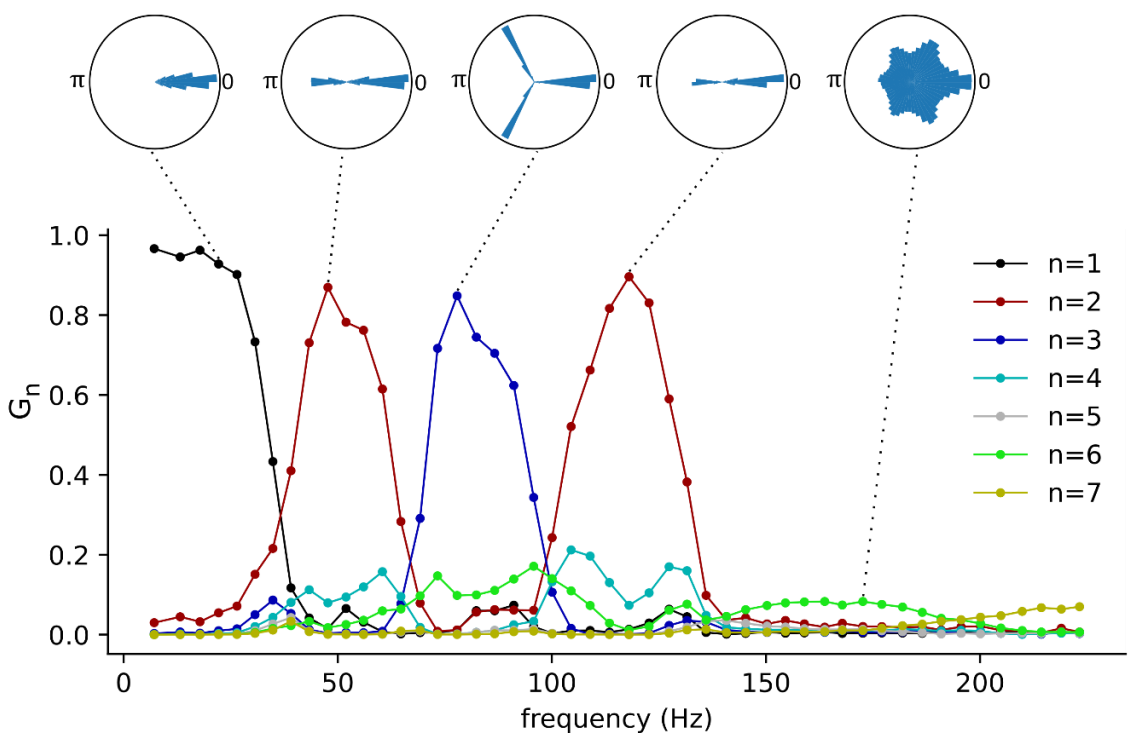

Figure 2. The network-wide stability and the number of phase clusters in the fast-spiking neurons as functions of pyramidal neuron frequency. Polar histograms show phase differences ϕ_j for all pairs of neurons in representative networks. Pyramidal neuron frequency was computed by taking the inverse of the average population interspike intervals.

Results

The simulated network model incorporates a significant difference in the spiking time scales of the pyramidal and fast-spiking interneurons. The slower excitatory drive from the pyramidal neurons modulates the fast-spiking dynamics of the interneurons, resulting in bursting oscillations in the latter (**Fig. 1B&C**). The inhibitory interactions between these bursting neurons then leads to itinerant metastable behavior. That is, ongoing endogenous transitions occur between different phase-locked (attractor) states. An example is illustrated in **Fig. 1C**, which shows the bursting oscillations of a representative pair of neurons versus time. At first, the neurons are locked in phase, but then they transition to an out-of-phase state. After a short time, they return to the in-phase state, and then switch back to the out-of-phase state. Similar persistent behavior was described in a previous report (Venkadesh et al., 2020).

The frequency of pyramidal neuron spiking is determined by the value of I^{ext}. To examine the effect of this driving frequency on the characteristics of metastability in the fast-spiking interneuron network, we systematically varied I^{ext} and measured the distribution of phase differences (ϕ_j) between pairs of interneurons as described in Methods. **Fig. 2** shows a plot of G_n (n=1, 2, …, 7), which quantifies the degree to which the interneuron phase differences group into n clusters, versus the pyramidal neuron spiking frequency (f). Above the plot are polar histograms of the phase differences (ϕ_j) for selected f's. At low driving frequency, all the inhibitory neurons lock in-phase, and thus their phase differences are close to zero. Correspondingly, G_1 is high and G_2 through G_7 are low. Interestingly, as the driving frequency is increased beyond ~25Hz, clusters appear in the phase difference distribution. We find that a well-defined state of two clusters

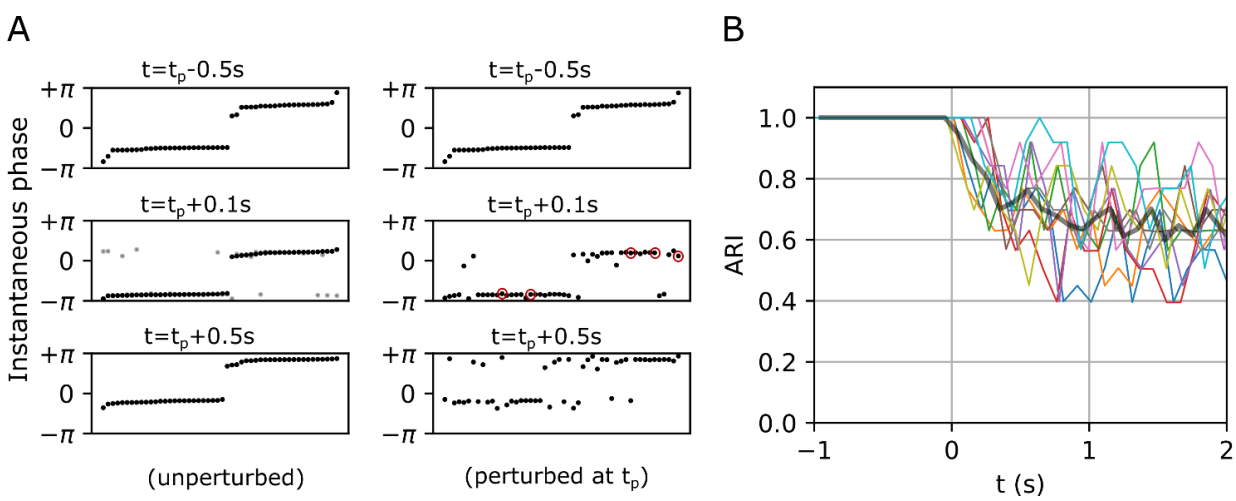

Figure 3. Exogenous transitions in the fast-spiking population. **A.** Left and right panels show the temporal evolution of a network in unperturbed and perturbed conditions respectively. Neurons (black dots) in the left panels are sorted by their instantaneous phases, and their order is preserved in the right panels for each t to show the divergence of states caused by perturbation (Endogenous transitions are shown in the left middle panel by the grey dots that preserve the sorted order from the left top). $t_p$denotes the time of perturbation, and red circles in the right middle panel denote perturbed neurons. **B.** Ten representative ARI curves (color) computed by comparing cluster assignments of neurons between unperturbed and perturbed conditions. The black curve represents the average. Here, t=0 corresponds to the perturbation times.

emerges near f =50Hz, and a three-cluster state emerges near f =80Hz. As the driving frequency is further increased, the pattern reverses and another well-defined state of two clusters appear near f =120Hz. Beyond f =140Hz, all G_n are small and the phase difference distributions become more uniform. It is interesting to note that the emergence of these clustered states occurs for driving frequencies within the gamma range [25Hz, 140Hz]. Pyramidal neurons are indeed known to fire at gamma frequencies, although such gamma cycles have been observed to be modulated by slower theta cycles (Dragoi & Buzsáki, 2006; O'Keefe & Recce, 1993). These results suggest that the metastable attractors emerge in the interneuron population when their spiking dynamics are appropriately driven by slower excitatory frequencies. Furthermore, our results show that the characteristics of the emergent metastability systematically depend on the frequency of oscillations.

The multi-clustered states described above exhibit spontaneous and endogenous itinerant dynamics. Motivated by the fact that an organism adapts its internal state to the environment via external stimuli, we sought to measure how a metastable state would be affected by an external perturbation. To do this, the network was simulated twice with identical initializations. The first simulation established the baseline dynamics as shown in **Fig. 3A** (left). The panels on the left show the instantaneous phases of the interneuron population at three times. The neurons are ordered along the horizontal axis by increasing phase. To mask the itinerant behavior, this ordering is performed separately for each panel. (Itinerant behavior is illustrated in the second panel, which shows in gray dots the phases of neurons that spontaneously switched relative to the top panel.) In the second simulation, an external perturbation was applied. Five randomly selected interneurons each received a single spike at time t_p. The results are shown in the panels of **Fig. 3A** (right). The time of perturbation occurred between the top and middle panels. Note that the neuron orderings from the left columns are preserved in the right columns. Thus, any differences in the cluster assignment of neurons

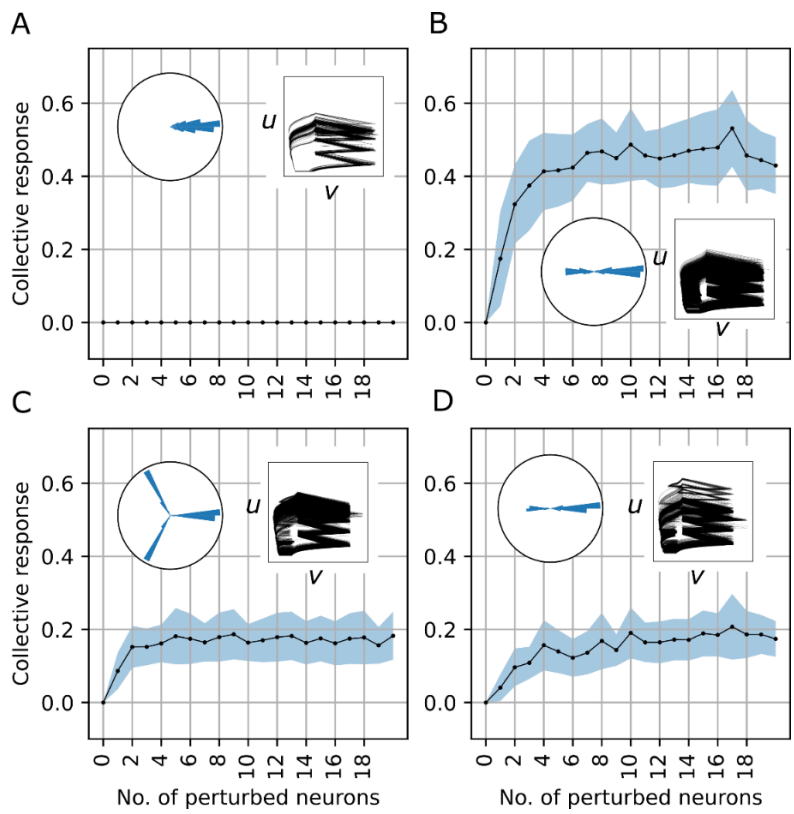

Figure 4. Dynamics of exogenous transitions characterized by cluster similarity over time for the four stable populations (A-D). A total of 50 perturbation experiments were performed for each number of perturbed neurons. Values represent means and shaded areas represent 99.9% confidence intervals. Insets show multi-stable phase clusters as polar histograms (left) and the phase portraits of all 50 neurons overlaid (right).

are due exclusively to the perturbation. Additionally, the transitions are collective in the sense that they occur in many non-perturbed neurons immediately following a small perturbation (**Fig. 3A** - right). This highlights the synergy of interacting elements in metastable networks. Collective transitions may be characterized by treating network states as multiple instantaneous phase clusters of neurons at any given time and subsequently comparing the cluster assignments of neurons between unperturbed and perturbed conditions using the ARI (**Fig. 3B**).

Next, we examined collective response features (Equation – 9) in the metastable networks that showed high magnitudes of stability. These are shown in **Fig. 4** along with the non-responsive single-clustered network (**Fig. 4A**). The metastable networks elicited collective responses in different magnitudes (**Fig. 4B-D**). However, the collective response reached a maximum in each metastable network as the number of perturbed neurons was increased. Interestingly, the two metastable networks that both exhibited two-clustered states showed very different collective response characteristics (**Fig. 4B&D,** also compare their phase portraits in right insets). Note that the excitatory frequency affects the inter-burst intervals in interneurons and consequently shapes their multi-periodic trajectories in the phase space (**Fig. 4** – right insets). Taken together, these results suggest that the metastability realized in the interneuron populations may arise from mechanisms (Ott et al., 1993; Sommerer & Ott, 1993; Tsuda, 2009) that evolve depending on the frequencies of excitatory oscillations within a cortical region.

Discussion

The spiking neural network model presented in this paper provides a compact mesoscopic scale approximation of regional dynamics that capture a crucial biological complexity at the level of individual neurons. A limitation of this model is that it only includes two types of neuron populations whereas intraregional neural circuits consist of populations with diverse frequency profiles (Komendantov et al., 2019). Nevertheless, this work suggests that the emergent metastability systematically depends on the spiking timescales of interacting neurons and provides a theoretical framework to unify populations of neurons with heterogenous frequency profiles. Furthermore, the model is easily scalable to study interregional interactions in the brain. Empirically estimated anatomical connectivity between brain regions could provide useful information for modeling interregional metastability. Note that while the model and the analyses presented in this study suggest a link between two temporal scales of network dynamics, modeling interregional interactions using their anatomical connectivity will further provide a venue to study metastable brain dynamics at a macroscopic spatial scale. In the next section, potential applications of the intraregional model are discussed by first addressing a challenge in whole-brain modeling and then discussing empirical observations of atypical brain physiology that can be mechanistically interpreted in whole-brain models.

Applications to whole-brain modeling and understanding the mechanisms of atypical brain physiology:

Sustained background activity in the cortex arises from the mutual excitation of excitatory neurons (Walter J. Freeman, 2008) such as the pyramidal neurons that project their axons to longer distances than the interneurons. Such long-distance projections are captured in diffusion-weighted

magnetic resonance imaging (dMRI) as white matter tracts. Estimation of anatomical connectivity from dMRI relies on the tractography-derived streamline counts between regions (Mori & van Zijl, 2002). However, the direction of axonal projections is not identifiable from the dMRI tractography. In other words, if the tractography estimates that there are *n* streamlines between regions A and B, the fraction of *n* that corresponds to the axonal projections from region A to B (and vice versa) is unidentifiable based on the tractography alone. The net excitatory input to a region is a key determinant of its firing frequency. Since the regional metastable dynamics may depend upon the frequency of excitatory oscillations (See **Figs. 2&4**), resolving the directionality of fiber tracts (i.e., incoming vs. outgoing for a region) will be important to accurately model the whole-brain metastable dynamics.

Previous whole-brain modeling studies considered symmetric couplings between pairs of brain regions and estimated a global coupling constant to supplement the connectivity information derived from white matter tractography (Deco & Jirsa, 2012; Deco et al., 2013). However, the unknown degrees of asymmetries in structural connections could be estimated for the whole brain, in principle, by numerical optimization. The network-wide stability of attractors (Equation – 6) realized across the frequency spectrum in whole-brain models could serve as a heuristic metric to search for the directionality, or more generally, the asymmetries in the bidirectionality, of macroscopic anatomical connections. Note that the number of unknown parameters is directly related to the spatial resolution of structural connectivity specification. It is uncertain if a model description at a high spatial resolution is solvable in practice due to the computational demands. However, models can be described at various spatial resolutions of a group-averaged whole-brain connectome, and the convergence patterns of optimization solutions for each spatial resolution can be examined. These convergence patterns should be compared against those of the null models with randomly shuffled anatomical connections. The robustness of the solution convergence relative to that of the respective null model can inform the preferred spatial resolution for the whole-brain models. This approach considers that the brain-wide features of the human connectome evolved to be highly specific, and they provide strong constraints to model network-wide transient attractor dynamics. The identified directionalities can also be validated against findings from the morphological tracing studies that report the directions of axonal projections between cortical regions using anterograde or retrograde tracing techniques (Foster et al., 2021).

The whole-brain models of anatomically constrained mesoscopic scale metastable dynamics are useful mathematical tools that will enable a multiscale understanding of cortical dynamics and illuminate neural network mechanisms of pathophysiology in neurological disorders. As an example, we briefly discuss how a whole-brain model of metastable dynamics could be useful in elucidating the pathophysiology of Parkinson's disease (PD). The structural degeneration of cortical and subcortical connectivity is a key factor underlying the motor and cognitive deficits in PD (Atkinson-Clement et al., 2017; Cochrane & Ebmeier, 2013; McGregor & Nelson, 2019). However, the mechanisms by which the structural degeneration alters the brain-wide dynamics in PD is not well understood. A whole-brain model of metastable dynamics constrained by the PD-affected anatomical connectivity can potentially delineate such mechanisms. For instance, amplified synchronization in beta frequency (8Hz – 30Hz), which has been reported in the cortical and basal ganglia circuits of PD subjects, is hypothesized to contribute to PD symptoms (Brittain

et al., 2014; Hammond et al., 2007; McGregor & Nelson, 2019). In particular, longer episodes of beta oscillations in the subthalamic nucleus (STN) (Deffains et al., 2018) and its higher synchronization with the cortical supplementary motor area (SMA) were associated with the freezing of gait in PD (Toledo et al., 2014). It may be hypothesized that the freezing of gait in PD is contributed by a reduction in synergistic transitions between different attractor states realized in these areas. The increased beta synchronization between STN and SMA observed in PD, and the hypothesized reduction in attractor transitions can be validated in whole-brain models by examining their stability (Equation – 6) and collective response characteristics (Equation – 9) respectively. Furthermore, by selectively targeting frequency bands for manipulation, one can investigate causal relationships between specific frequencies of oscillations and the dynamics of transitions between attractor states realized across multiple timescales. Such whole-brain models could also enable identification of network mechanisms to restore optimal brain dynamics in PD and other neurological disorders.

Conclusion:

The numerical simulations in this study show that the inhibitory interneuron oscillations that are modulated by slower excitatory neurons, under specific conditions, realize metastable attractors. Furthermore, our analyses revealed frequency dependences of the emergent metastability and quantitatively associated the features of spiking neural network dynamics at two temporal scales. This novel cross-timescale association using a compact mathematical description captures a biological complexity of neural circuits at the level of individual neurons and allows, in principle, a scalable integration with empirical observations of neural network features to develop a coherent understanding of nervous system functions.

Acknowledgments:

The authors thank Alev Erisir, Giselle Petzinger, Michael Jakowec, and Dawn Schiehser for their insights and helpful discussions. The authors appreciate the complementary perspectives of Jeffrey Kopsick, Giorgio Ascoli, and Alexander Komendantov and are thankful for their many valuable discussions.

Author Contributions:

SV and JDVH conceptualized the study. SV and AS performed analyses. EB, HS, and TRH provided critical inputs at various stages of this study. SV and EB wrote the manuscript. JDVH supervised the study and was responsible for funding acquisition.

Declaration of Interests:

The authors declare that they have no known competing financial interests or personal relationships that could have appeared to influence the work reported in this paper.

Funding:

This work was supported in parts by the Department of Defense grant W81XWH 18 1 0665 PD170037 and an internal funding from the University of Virginia.

References:

Atkinson-Clement, C., Pinto, S., Eusebio, A., & Coulon, O. (2017). Diffusion tensor imaging in Parkinson's disease: Review and meta-analysis. *NeuroImage. Clinical*, *16*, 98–110.

Brittain, J.-S., Sharott, A., & Brown, P. (2014). The highs and lows of beta activity in cortico-basal ganglia loops. *The European Journal of Neuroscience*, *39*(11), 1951–1959.

Cabral, J., Castaldo, F., Vohryzek, J., Litvak, V., Bick, C., Lambiotte, R., Friston, K., Kringelbach, M. L., & Deco, G. (2022). Metastable oscillatory modes emerge from synchronization in the brain spacetime connectome. *Communications Physics*, *5*(1), 1–13.

Cochrane, C. J., & Ebmeier, K. P. (2013). Diffusion tensor imaging in parkinsonian syndromes: a systematic review and meta-analysis. *Neurology*, *80*(9), 857–864.

Daido, H. (1996). Onset of cooperative entrainment in limit-cycle oscillators with uniform all-to-all interactions: bifurcation of the order function. In *Physica D: Nonlinear Phenomena* (Vol. 91, Issues 1–2, pp. 24–66). https://doi.org/10.1016/0167-2789(95)00260-x

Deco, G., & Jirsa, V. K. (2012). Ongoing cortical activity at rest: criticality, multistability, and ghost attractors. *The Journal of Neuroscience: The Official Journal of the Society for Neuroscience*, *32*(10), 3366–3375.

Deco, G., Ponce-Alvarez, A., Mantini, D., Romani, G. L., Hagmann, P., & Corbetta, M. (2013). Resting-state functional connectivity emerges from structurally and dynamically shaped slow linear fluctuations. *The Journal of Neuroscience: The Official Journal of the Society for Neuroscience*, *33*(27), 11239–11252.

Deffains, M., Iskhakova, L., Katabi, S., Israel, Z., & Bergman, H. (2018). Longer β oscillatory episodes reliably identify pathological subthalamic activity in Parkinsonism. *Movement Disorders: Official Journal of the Movement Disorder Society*, *33*(10), 1609–1618.

Dragoi, G., & Buzsáki, G. (2006). Temporal encoding of place sequences by hippocampal cell assemblies. *Neuron*, *50*(1), 145–157.

Ego-Stengel, V., & Wilson, M. A. (2007). Spatial selectivity and theta phase precession in CA1 interneurons. *Hippocampus*, *17*(2), 161–174.

Foster, N. N., Barry, J., Korobkova, L., Garcia, L., Gao, L., Becerra, M., Sherafat, Y., Peng, B., Li, X., Choi, J.-H., Gou, L., Zingg, B., Azam, S., Lo, D., Khanjani, N., Zhang, B., Stanis, J., Bowman, I., Cotter, K., … Dong, H.-W. (2021). The mouse cortico-basal ganglia-thalamic network. *Nature*, *598*(7879), 188–194.

Freeman, W. J. (1999). Consciousness, intentionality and causality. *Journal of Consciousness Studies*. https://www.ingentaconnect.com/content/imp/jcs/1999/00000006/F0020011/995

Freeman, Walter J. (2008). A pseudo-equilibrium thermodynamic model of information processing in nonlinear brain dynamics. *Neural Networks: The Official Journal of the International Neural Network Society*, *21*(2–3), 257–265.

Frégnac, Y. (2017). Big data and the industrialization of neuroscience: A safe roadmap for understanding the brain? *Science*, *358*(6362), 470–477.

Golomb, D., & Hansel, D. (2000). The number of synaptic inputs and the synchrony of large, sparse neuronal networks. *Neural Computation*, *12*(5), 1095–1139.

Hammond, C., Bergman, H., & Brown, P. (2007). Pathological synchronization in Parkinson's disease: networks, models and treatments. *Trends in Neurosciences*, *30*(7), 357–364.

Hubert, L., & Arabie, P. (1985). Comparing partitions. *Journal of Classification*, *2*(1), 193–218.

Izhikevich, E. M. (2003). Simple model of spiking neurons. *IEEE Transactions on Neural Networks / a Publication of the IEEE Neural Networks Council*, *14*(6), 1569–1572.

Jones, M. W., & Wilson, M. A. (2005). Phase precession of medial prefrontal cortical activity relative to the hippocampal theta rhythm. *Hippocampus*, *15*(7), 867–873.

Komendantov, A. O., Venkadesh, S., Rees, C. L., Wheeler, D. W., Hamilton, D. J., & Ascoli, G. A. (2019). Quantitative firing pattern phenotyping of hippocampal neuron types. *Scientific Reports*, *9*(1), 17915.

Kopsick, J. D., Tecuatl, C., Moradi, K., Attili, S. M., Kashyap, H. J., Xing, J., Chen, K., Krichmar, J. L., & Ascoli, G. A. (2022). Robust Resting-State Dynamics in a Large-Scale Spiking Neural Network Model of Area CA3 in the Mouse Hippocampus. *Cognitive Computation*. https://doi.org/10.1007/s12559-021-09954-2

Lisman, J. (2005). The theta/gamma discrete phase code occuring during the hippocampal phase precession may be a more general brain coding scheme. *Hippocampus*, *15*(7), 913–922.

Markram, H., Muller, E., Ramaswamy, S., Reimann, M. W., Abdellah, M., Sanchez, C. A., Ailamaki, A., Alonso-Nanclares, L., Antille, N., Arsever, S., Kahou, G. A. A., Berger, T. K., Bilgili, A., Buncic, N., Chalimourda, A., Chindemi, G., Courcol, J.-D., Delalondre, F., Delattre, V., … Schürmann, F. (2015). Reconstruction and Simulation of Neocortical Microcircuitry. *Cell*, *163*(2), 456–492.

McGregor, M. M., & Nelson, A. B. (2019). Circuit Mechanisms of Parkinson's Disease. *Neuron*, *101*(6), 1042–1056.

Mori, S., & van Zijl, P. C. M. (2002). Fiber tracking: principles and strategies - a technical review. *NMR in Biomedicine*, *15*(7–8), 468–480.

O'Keefe, J., & Recce, M. L. (1993). Phase relationship between hippocampal place units and the EEG theta rhythm. *Hippocampus*, *3*(3), 317–330.

Ott, E., Sommerer, J. C., Alexander, J. C., Kan, I., I., & Yorke, J. A. (1993). Scaling behavior of chaotic systems with riddled basins. *Physical Review Letters*, *71*(25), 4134–4137.

Pedregosa, F., Varoquaux, G., Gramfort, A., Michel, V., Thirion, B., Grisel, O., Blondel, M., Prettenhofer, P., Weiss, R., Dubourg, V., Vanderplas, J., Passos, A., Cournapeau, D., Brucher, M., Perrot, M., & Duchesnay, É. (2011). Scikit-learn: Machine Learning in Python. *Journal of Machine Learning Research: JMLR*, *12*(Oct), 2825–2830.

Poe, G. R., Nitz, D. A., McNaughton, B. L., & Barnes, C. A. (2000). Experience-dependent phase-reversal of hippocampal neuron firing during REM sleep. *Brain Research*, *855*(1), 176–180.

Rand, W. M. (1971). Objective Criteria for the Evaluation of Clustering Methods. *Journal of the American Statistical Association*, *66*(336), 846–850.

Skaggs, W. E., & McNaughton, B. L. (1996). Replay of neuronal firing sequences in rat hippocampus during sleep following spatial experience. *Science*, *271*(5257), 1870–1873.

Sommerer, J. C., & Ott, E. (1993). A physical system with qualitatively uncertain dynamics. *Nature*, *365*(6442), 138–140.

Steinley, D. (2004). Properties of the Hubert-Arable Adjusted Rand Index. *Psychological Methods*, *9*(3), 386–396.

Stimberg, M., Brette, R., & Goodman, D. F. (2019). Brian 2, an intuitive and efficient neural simulator. *ELife*, *8*. https://doi.org/10.7554/eLife.47314

Tognoli, E., & Kelso, J. A. S. (2014). The metastable brain. *Neuron*, *81*(1), 35–48.

Toledo, J. B., López-Azcárate, J., Garcia-Garcia, D., Guridi, J., Valencia, M., Artieda, J., Obeso, J., Alegre, M., & Rodriguez-Oroz, M. (2014). High beta activity in the subthalamic nucleus and freezing of gait in Parkinson's disease. *Neurobiology of Disease*, *64*, 60–65.

Tsuda, I. (2009). Hypotheses on the functional roles of chaotic transitory dynamics. *Chaos* , *19*(1), 015113.

Venkadesh, S., Barreto, E., & Ascoli, G. A. (2020). Itinerant complexity in networks of intrinsically bursting neurons. *Chaos* , *30*(6), 061106.

Venkadesh, S., & Van Horn, J. D. (2021). Integrative Models of Brain Structure and Dynamics: Concepts, Challenges, and Methods. *Frontiers in Neuroscience*, *15*, 752332.

Vinck, M., Lima, B., Womelsdorf, T., Oostenveld, R., Singer, W., Neuenschwander, S., & Fries, P. (2010). Gamma-phase shifting in awake monkey visual cortex. *The Journal of Neuroscience: The Official Journal of the Society for Neuroscience*, *30*(4), 1250–1257.